Contents

5. Materials and Techniques for Spacecraft* Static Charge Control

L.J. Amore and A.E. Eagles
General Electric Company
Space Division
Valley Forge, Pennsylvania

Abstract

An overview of the design, development, fabrication, and testing of transparent conductive coatings and conductive lattices deposited or formed on high resistivity spacecraft dielectric materials to obtain control static charge buildup on spacecraft external surfaces is presented.

Fabrication techniques for the deposition of indium/tin oxide coatings and copper grid networks on Kapton and FEP Teflon films and special frit coatings for OSR and solar cell cover glasses are discussed. The techniques include sputtering, photoetching, silkscreening, and mechanical processes.

A facility designed and built to simulate the electron plasma at geosynchronous altitudes is described along with test procedures. The results of material characterizations as well as electron irradiation aging effects in this facility for spacecraft polymers treated to control static charge are presented. The data presents results for electron beam energies up to 30 kV and electron current densities of 30 nA/cm^2. Parameters measured include secondary emission, surface leakage, and through the sample currents as a function of primary beam energy and voltage.

*This work was supported by the Air Force Materials Laboratory under Contracts F33615-76-C-5075 and F33615-76-C-5258.

1. INTRODUCTION

The primary means for maintaining reasonable operating temperatures within a spacecraft is by discretely adjusting the amount of energy absorbed from the sun and the amount that is radiated at the infrared wavelength corresponding to the local surface temperature. This technique is known as passive temperature control and is highly dependent on the reflective and emissive properties of the materials located on the external surfaces. Surface temperatures and subsequently the overall spacecraft equilibrium temperature can be adjusted using active or semiactive techniques such as louvers that are opened and closed to effectively change the reflective and emissive properties in the louver area. Heat pipes have been used to move internally generated heat to the surface where it can be radiated efficiently to space.

To achieve passive thermal control, dielectric insulating materials must necessarily be used, because only these materials have the combination of inherent high solar reflectance and high emittance required for acceptable thermal balance. This class of materials includes back surface aluminum and silver coated FEP Teflon films, high purity silica glass thermal control materials, and Kapton and Mylar films used in multilayer insulation blankets.

In geosynchronous orbit these dielectric materials are directly exposed to bombardment by the indigeneous electron plasma. As electrical insulators they support charge buildup until dielectric breakthrough or arcing to areas or components of lower potential occurs. The results of these incidents include degradation of material, thermo-optical, and mechanical properties and disruption of components operating at radio frequencies by the electromagnetic noise generated by an arc.

The purpose of this study is to develop materials and techniques to control static charge buildup on conventional spacecraft coatings and materials for use during geosynchronous orbit satellite missions. This study represents the progress made during the first six months of a planned 24-month program. The results are preliminary, but significant progress has been made to indicate that transparent conducting oxide overlay coatings and conducting grids or screens placed over dielectric surfaces offer potential solutions to the problem.

The materials investigated thus far in the study include:

(1) Aluminized FEP Teflon films used extensively as a high emittance, solar reflecting second surface mirror thermal control coating,

(2) Back surface aluminized Kapton film used as a top layer for multilayer insulation blankets,

(3) Optical Solar Reflecting (OSR) tiles which perform similar to the FEP film coating described above, but consisting of an 8 mil thick slice of 7940 Silica glass with a back surface coating of silver, then Inconel, to produce a second surface mirror, and

(4) Glasses, such as Corning 7940 and microsheet used to cover silicon solar cells.

2. MATERIALS TESTING

2.1 Philosophy and Approach to Static Charge Control Testing

In a materials development program fundamental material parameters are of major importance, because as materials are developed and observed in a simulated space environment it is necessary to identify those characteristics responsible for the observed behavior. With this in mind a facility was developed which could both observe behavior in a simulated environment and then perform the fundamental measurements associated with surface phenomena. If we can identify the location and motion of all charged particles within a closed system we will be well on the way to identifying and defining the processes taking place on and within the material being studied.

In meeting this objective it is necessary to know the flux, energy distribution, and spatial distribution of the flood gun beam so all charges arriving at the surface under test are known. It is required to have a secondary charged-particle collector to identify and quantize all charges leaving the surface and means of measuring the current diffusing through the surface to the substrate upon which the sample has been mounted. Lastly, a capability is needed to measure that charge which is residing on the surface itself.

Another important consideration is in simulating the high pumping speed within the closed system that an exposed surface in deep space would see. Here pumping speed is more important than ultimate pressure as a material under particle bombardment will evolve gas resulting in a high pressure very close to the surface. At localized pressures around 10^{-3} Torr or higher, discharge phenomena not common to a deep space environment will occur and could result in improper conclusions during experimental work. These problems are alleviated only through a system with very high pumping speed in pressure regions greater than 10^{-4} Torr. Vacion and vacion triode pumps cannot pump efficiently at pressures greater than 10^{-4} Torr to 10^{-1} Torr. Augmented diffusion pumps on the other hand have their peak pumping speed between 10^{-4} and 10^{-2} Torr. By placing a booster in the foreline of a 500-l/sec diffusion pump, its speed can be increased up to 2500 l/sec in the critical region between 10^{-4} and 10^{-2} Torr.

2.2 Electrostatic Discharge (ESD) Test Facility

Using the criteria established in the previous section a system was designed and built at GE. The system is shown schematically in Figure 1 and in the photographs

of Figure 2. The chamber is large enough to provide adequate pumping volume and room to work inside through large access ports when placing and adjusting samples for evaluation.

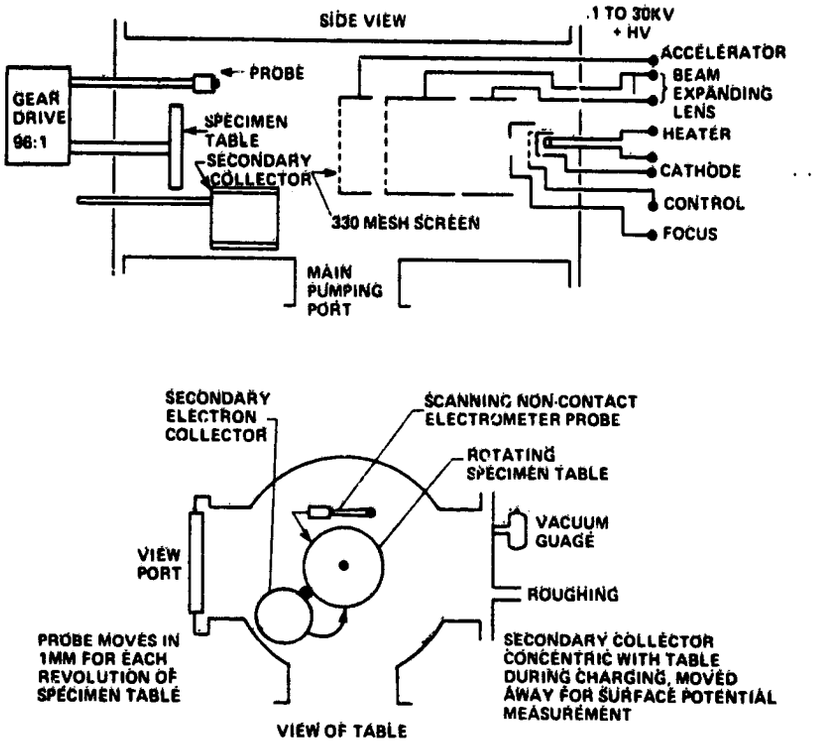

Figure 1. Functional Diagram of ESD Test Facility

At the heart of the facility is the electron flood gun which is used to simulate the space environment with respect to charged particle bombardment. It should be noted that this facility does not make provisions for ion and proton bombardment; however, Knott[1] and others have shown that these do not significantly affect spacecraft charging, since they have a lower probability of striking the spacecraft. The electron flood gun was designed to simulate the electron environment measured at ATS-5 as modified by more recent data from ATS-6. The design of the gun includes an electrostatic, three-element lens to assure uniform beam expansion in the restricted space of the chamber, control grids which can be modulated to simulate the measured electron energy distribution, and a wide range of adjustment in flux density.

The specimen diagnostic assembly is mechanically the most complicated subassembly but it has great versatility for the measurement of fundamental properties.

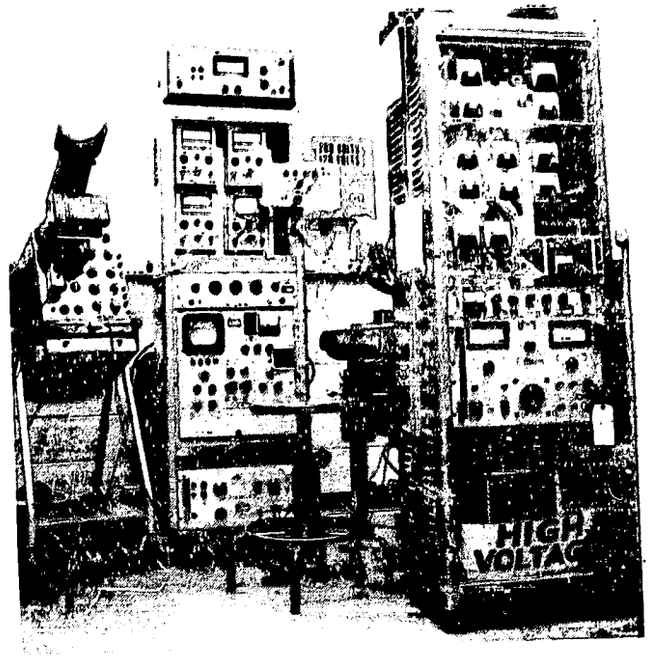

a. Associated Diagnostic Equipment

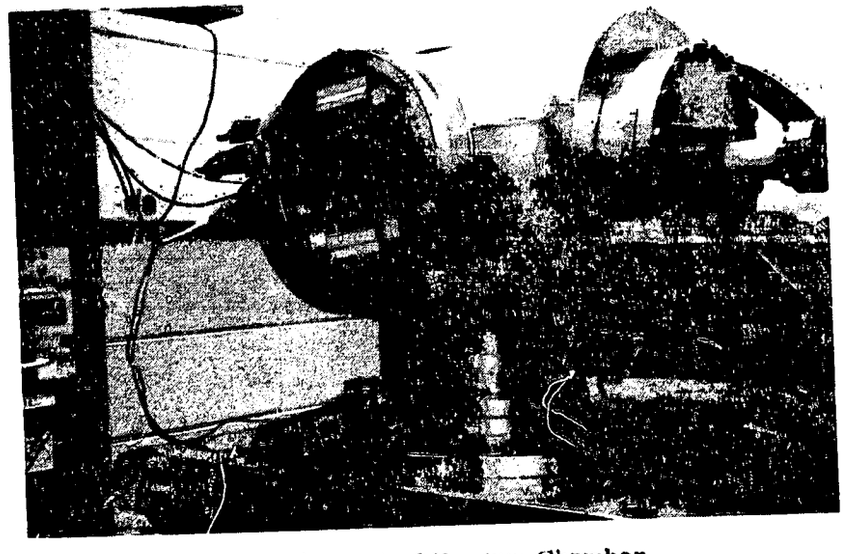

b. Close-up of Vacuum Chamber

Figure 2. ESD Facility

It consists of an electrically isolated rotating table for holding specimens up to a 5-in. diameter. By measuring the current flowing through the table the diffusion current through the specimen may be monitored. A non-contact surface potential probe is mounted on a movable arm which is connected through a gear box to the rotating table. The gear ratio is such that for every rotation of the table the probe arm is advanced in millimeter steps allowing the probe to track the surface of the sample much like a tone arm tracks a record on a phonograph. This motion is driven by a dc reversible electric motor which is also coupled to a resistance commutator for driving one axis of an X-Y recorder. A Monroe model 144 probe is used that has high resolution and is relatively independent of probe-to-surface distance. The electronics incorporates a phase-lock loop amplifier for the reduction of spurious/pick-up, and noise. During the bombardment phase of the tests this probe can be swung completely out of the way so no part of it will shadow the sample during charging.

A secondary electron collector ring is also part of the assembly which is swung in place around the sample during the charging phase and it is used to monitor charged particles leaving the surface of the sample. By pulsing the flood gun beam it can also measure the secondary emission ratio of the specimen under test. With slight modification this electrode may also be used to monitor surface erosion products during charging similar to the experiments performed by Nanewicz[2] of Stanford Research Institute.

3. APPROACHES TO THE PROBLEM

3.1 Transparent Oxides

The most commonly used transparent conductive coatings are combinations of indium and tin oxides (ITO) or indium oxide, doped with fluorine or antimony. These coatings were first developed for heating canopies of aircraft, transparent back conductors for liquid crystal displays.

The techniques for depositing these materials onto varied geometries has mushroomed over the past four years, varying from vacuum vapor deposition, chemical vapor deposition, dc sputtering, RF diode sputtering, and magnetron sputtering techniques.

The one primary objective in depositing transparent conductors of metallic oxides is to closely control the doping cations or oxygen vacancies. Over oxidation causes the film to be highly electrically resistive. Under oxidation causes the film to be highly metallic or brown; the proper balance of oxygen pressure during evaporation results in a coating that is transparent and conductive.

The electrical conductivity of sputtered ITO films decrease as the partial pressure of oxygen rises beyond 1×10^{-5} as can be seen in Figure 3. This data was taken from measurements using RF diode sputtered films of ITO on microsheet substrates. Recent results using magnetron sputtering where the glass surface is cool during deposition have also supported the ITO coatings dependence on partial pressure of oxygen.

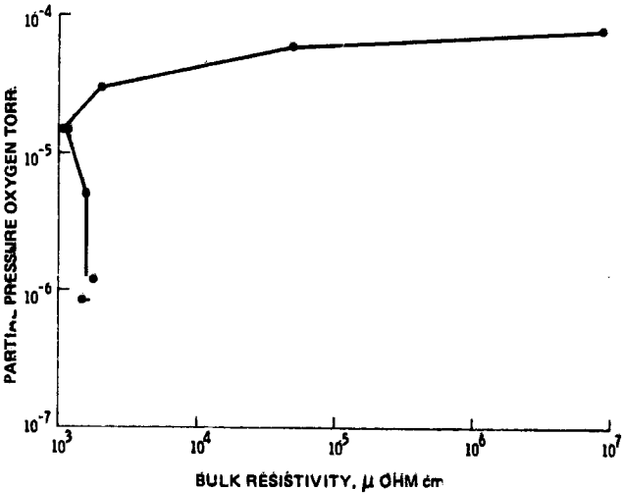

Figure 3. Resistivity of Sputtered Indium Oxide/Tin Oxide Films

ITO and indium films were prepared on Kapton and FEP by conventional vapor deposition from a crucible source, dc coaxial sputtering and magnetron sputtering. All techniques have been successful for ESD applications and Table 1 shows the base variations in surface resistivities obtained from three different techniques.

Based on measurements to date, 250 Å of ITO have measurable but no catastrophic effect on α/ϵ characteristics of films. Tables 2 and 3 give electrical and optical data for ITO films deposited by sputtering techniques on FEP and Kapton thin film substrates.

Other conductive variations of semiconductor coatings are currently being considered such as cadmium stannate and also variations of aluminum oxide and oxides of chrome.

Table 1. Surface Resistivities of 100 Å Films Deposited by Various Techniques

	Coaxial	Magnetron	In_2O_3 Filament
Kapton	100 K	7.9 K	5×10^7
FEP	200 K	7.9 K	5×10^7
Microsheet Coverglass	90 K	7.9 K	5×10^7

Table 2. Electrical and Optical Characteristics 90% In_2O_3 / 10% (ITO) Coated FEP

FEP Thickness	Resistance kΩ/□	ITO Thickness, Å	(Visible) Transmission
0.002	76 - 318	250 ± 50	0.91
0.002	115 - 352	250 ± 40	0.90
0.005	183 - 450	250 ± 50	0.87
0.002	5.16 - 21.3	500 ± 50	0.80
0.002	9.2 - 35.3	500 ± 50	0.81
0.002	27 - 48.1	500 ± 50	0.81
0.005	8.1 - 52.3	500 ± 50	0.80
0.005	46 - 86	900 ± 50	0.77
0.005		Uncoated	0.94
0.002		Uncoated	0.95

Table 3. Electrical and Optical Characteristics 90% In_2O_3 / 10% SnO_2 (ITO) Coated Kapton (2 mil)

ITO Thickness, Å	Resistivity kΩ/□	(Visible) Transmission
900	0.45 - 0.75	56.6
900	0.45 - 0.75	53.1
500	3 - 7	59.4
500	3 - 7	58.7
250	80 - 150	59.9
250	80 - 150	59.9
Uncoated	10^{10}	60.0

3.1.1 PRELIMINARY SCANNING ELECTRON MICROSCOPE (SEM) ANALYSIS OF KAPTON AND ITO COATED KAPTON

Surface characteristics of Kapton and ITO coated Kapton were observed with an electron microscope at 10,000× (see Figures 4, 5, and 6). Figure 4 reveals a uniform Kapton surface with no evidence of imperfections. Figure 6 reveals a surface that underwent severe flexing (180° bend) with subsequent micro-fracturing of the film. This defect did not affect the conductivity of the film under electron beam bombardment as will be described later.

Figure 4. Uncoated Kapton Surface (at 10,000×)

Figure 5. Kapton Coated with 500 Å of ITO (at 10,000×)

Figure 6. Microcracks in 500 Å ITO Coating on Kapton After Severe Flexing (180° Bend) (at 10,000×)

3.2 Conductive Grids

Conductive lattices were prepared by various techniques on Kapton, Teflon, and Mylar. A summary of the work follows.

3.2.1 PHOTOETCHING

General Electric's standard microcircuit photoetching techniques were used to form grid patterns on copper coated Kapton substrates. In our first trial a 1/2-in. pattern was successfully obtained having a line pattern 0.015 in. wide and 1000 Å thick. The techniques allow processing of line patterns as thin as 0.001 in. and thicknesses in the 100 to 200 Å range. The copper lattice on Kapton film shown in Figure 7 was prepared by the following process:

(1) Art work is generated to produce the desired grid pattern,
(2) The art work is photo-reduced to the desired dimensions and a negative is produced,
(3) An appropriate thickness of copper is vapor deposited on the dielectric film,
(4) Photo-resist is deposited on the copper coating,
(5) The negative is placed over the photo-resist and is illuminated with ultra-violet radiation,
(6) The UV exposed pattern is placed in a developing solution and then baked at 120°F,
(7) The developed pattern is rinsed in aqueous solution to remove the developed photo-resist leaving the desired pattern which is then:
    (a) flushed with alcohol and dried,
    (b) etched in chromic acid,
    (c) rinsed with water, and
    (d) rinsed with MEK or trichloroethylene.

3.2.2 PYRALUX FOIL

Grids on Kapton films of thicknesses greater than 0.003 in. up to 0.015 in. can be photoetched from DuPont's Pyralux, thin foil copper clad Kapton. This material is formed using a process whereby the surface of the Kapton undergoes an activation process which permits laminating the Kapton surface with copper and results in a well adhering laminate. These clads are reported to be used where fine lines and spacings are required. Etched edges are sharper than those resulting from thin film etching, thus minimizing field emission problems resulting from feathered edges, under electron bombardment.

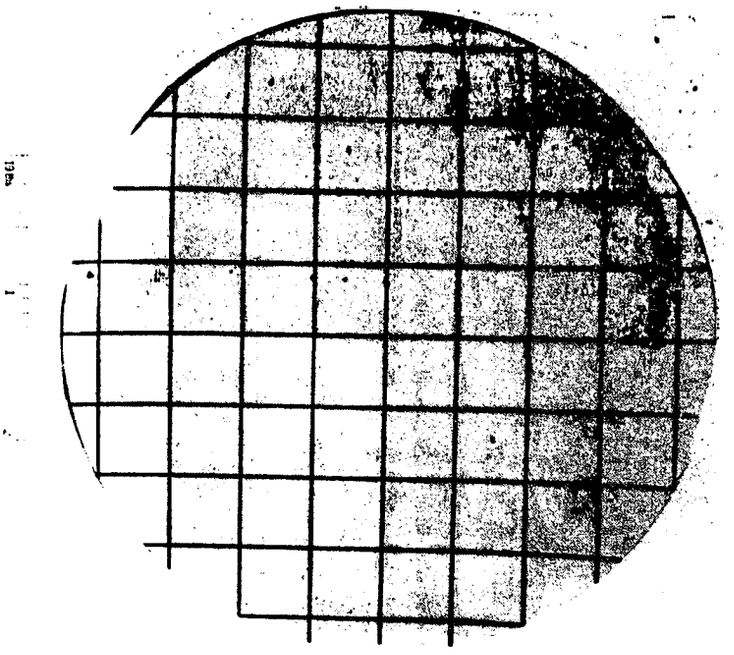

Figure 7. Photoetched Copper Lattice on Kapton

3.2.3 MESH IMBEDMENT

The challenge to laminate fine wire mesh into FEP has been a most difficult one. Initial samples appeared to have all the proper mechanical characteristics except aluminum wire bond disrupted during flexure testing. Current tests indicate that meshes of zinc, nickel, or silver attain a superior FEP to metal bond.

Mesh material laminated into FEP thus far have yielded bond strengths only up to 2 lb/inch.

3.2.4 SILK SCREENING TECHNIQUES

Silk screening masks with pitch varying from 3/8 to 3/4 in. have been fabricated. A silver epoxy screening material, No. 11095, manufactured by Electro-science Laboratories, Pennsauken, New Jersey, appears to be very promising. The process for silk screening is not anticipated to present a problem. It offers potential as a conductive surface for ground strap connections, for mechanical interconnects and as a solderable surface.

3.3 OSR and Solar Cell Cover Glass Modification

Four coatings were investigated for glass modification. One was alumino-germanoborate glass modified with oxides of zinc, lead, and lithium. Another

was a lithium borosilicate modified with oxides of lanthanum, tantalum, zinc, and cerium. The other two were commercially available aqueous potassium silicates. The coatings were applied to Pyrex glass coupons about 0.75 in. × 0.76 in. × 0.010 inch. Transmittance data were obtained on all of the specimens. Surface resistivity data were obtained for all specimens except the lithium borosilicate coating.

The aluminogermanoborate and lithium borosilicate glasses were developed several years ago under AFML Contract F3316-71-C-1656. The former was designated GE-5973-8; the latter is GE-1TL. Both were selected for the current program because of their very good transmission and resistance to beta irradiation. Very fine particles (~ 10 μ) of each glass were suspended in isopropyl alcohol and the slurry was gently poured onto a coupon of the Pyrex glass described previously.

After sufficient time for a sedimented layer to form, the excess slurry is siphoned off, the coated Pyrex coupon is dried and then fired at 550°C for times which vary with the composition. Usually, a time between 5 and 10 min is sufficient to bond the glass particles to each other and to the pyrex coupon. Subsequent examination revealed no stresses on the coated Pyrex compared to an uncoated Pyrex coupon.

*Kasil No. 1 and *Kasil No. 6, the aqueous potassium silicates, are proprietary, trademark registered products of the Philadelphia Quartz Company. The No. 1 material has a K_2O/SiO_2 ratio of 1:2.5; the No. 6 material has a K_2O/SiO_2 ratio of 1:2.1. Both silicates are commercially available as liquids which can be applied as thin coatings by spraying, brushing or dipping.

Kasil No. 1 and Kasil No. 6, as received from the manufacturer, were applied to the Pyrex coupons. In addition, Kasil No. 1 was modified with 0.5 percent CeO_2 and applied to Pyrex coupons. In all cases, the silicate coatings were dried at 100°C for two hours.

The transmittance of uncoated Pyrex and each of the uncoated specimens is shown in Figure 8. Examination of this data reveals that in the wavelength region of 0.3 to about 1.7 μ there is very little difference in transmission between the uncoated Pyrex and the silicate-coated Pyrex specimens. In the same range of wavelengths, the aluminogermanoborate coated Pyrex specimens exhibit slightly less transmission than the control specimen. The lithium borosilicate coated Pyrex transmission is identical to that of the uncoated control sample throughout the measurement spectrum, except for a slight absorption (due probably to the OH radical) at about 3.6 μ. The difference in transmission for the two 5973-8 coated specimens is due to the difference in thickness of the coatings. One (No. 2 specimen) is 0.4 mil thick; the other (No. 3 specimen) is 0.6 mil thick which represent a 50 percent increase in coating thickness. Electrical resistivity data shown in Table 4 indicates that this property is significantly reduced by all of the coatings with the aqueous silicate coatings having the greatest effect.

*Kasil is a trademark of Philadelphia Quartz Co.

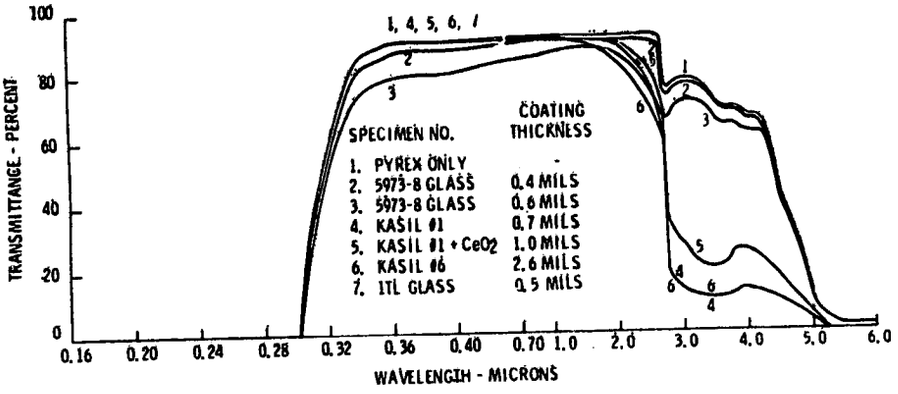

Figure 8. Transmittance of Coated and Uncoated 10-mil Pyrex Coupons

Table 4. Electrical Resistivity of Frit Coated Glasses

Specimen No.	Coating	Coating Thickness (Mils)	Electrical Resistivity ($\Omega/\square$)
1	None	None	10^9
2	5973-8 Glass	0.4	6.0×10^8
3	5973-8 Glass	0.6	4.0×10^8
4	Kasil No. 1	0.7	3.2×10^6
5	Kasil No. 1 CeO_2	1.0	8.0×10^6
6	Kasil No. 6	2.6	6.0×10^6
7	ITL Glass	0.5	5.0×10^8

4. BASELINE DATA: RESULTS OF SCREENING TESTS

The initial phase of this program was concerned with establishing the performance level of some typical spacecraft materials. The simulated space tests were conducted in the facility described previously. These tests established the onset of discharging for the four materials listed in Table 5 at a current density of 30 nA/cm^2. The point of discharge was determined visually in a darkened room. The qualitative data collected is typified in the photograph of Figure 9, which shows arcing along the edges of the 1×1 in. tiles in the OSR mosaic.

Table 5. Summary of Static Charging Screening Tests at 30 nA/cm^2

Material	Onset of Discharging, kV
Kapton, 2 mil - back surface aluminized	12 - 15
FEP Teflon, 5 mil - back surface silvered	20
Optical Solar Reflecting (OSR) coating mosaic	12
Solar Array Composite, 0211 microsheet over 2 × 2 cm cells	12

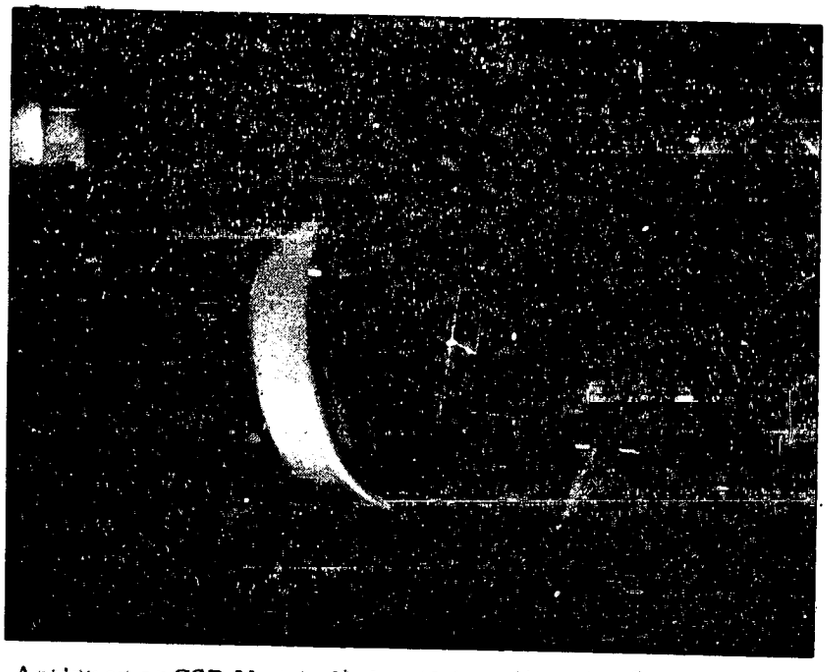

Figure 9. Arcing on an OSR Mosaic Under 15 kV - 30 nA/cm^2 Electron Bombardment

5. STATIC CHARGE TESTING

5.1 Introduction

Polymer materials were subjected to electron beam bombardment in the facility described previously. Results of the simulated environmental testing, which is performed in a vacuum of less than 10^{-6} Torr, are given in Table 5. Parameters normally measured during electron bombardment include: Primary beam current (I_P), surface leakage current (I_R), and backplate leakage (through the sample) current (I_L). The primary beam current as measured is the sum of the other currents, that is,

$$I_P = I_S + I_R + I_L .$$

Table 6. Summary of Static Charging Tests

Sample No.	Substrate	Back Surface Coating	Front Surface Coating	Observations	Conclusions
23 and 24	0.003" Mylar	None	None	Very large discharging occurring at 25 KV, 30 nA/cm^2 followed by quiescence lasting five minutes during which electro-luminescence prevailed	Unsatisfactory for static charge control.
26	0.005" FEP Teflon	None	250A° of 10 mole % SnO_2 in In_2O_3.	No discharges observed or recorded. Electro-luminescence observed through 25 KV, 30nA/cm^2.	Suitable for static charge control to at least 25 KV and 30 nA/cm^2.
27	0.002" Kapton	None	250A° of 10 mole % SnO_2 in In_2O_3.	No discharges observed or recorded. Electro-luminescence observed through 25 KV, 30 nA/cm^2.	Suitable for static charge control to at least 25 KV and 30 nA/cm^2.
28	0.002" FEP Teflon	None	Photoetched copper grid with 1/2 in. pitch. Copper filaments 0.015 in. wide x 3000A° thick.	At 15 KV, 30 nA/cm^2 clusters of electrical discharges occurred at a rate of 20 second within a 1 - in. diameter near center of sample. Other discharges occurred over entire 6 in. diameter surface randomly. Discharge amplitude to 200 nA.	Unsatisfactory performance. Probably due to poor bond between copper and FEP.
30	0.005" FEP Teflon	1000A° Vapor Deposited Aluminum	Same as Sample 28	Same performance as noted for Sample No. 28 except microscopic examination revealed some copper grid filaments to be broken.	Unsatisfactory performance. More intimate contact is needed between copper grid and FEP.
31	0.003" Kapton	None	Photoetched copper grid with 1/2 in. pitch. Copper filaments 0.015 in. wide x 0.003 in. thick copper applied to Kapton with DuPont Pyralux.	No discharges observed visually or by scope monitoring through (25 KV, 30 nA/cm^2. Some electro-luminescense observed.	Suitable for ESD control to at least 25 KV and 30 nA/cm^2.
32	0.001" Kapton	None	Silver Frit silk screened 1/2" pitch. Conductor .015" wide Frit material is Electroscience No. 11095.	No discharged observed visually or by scope monitoring (25 KV, 30 nA/cm^2)	Suitable for ESD control subject to mechanical and irradiation testing.

5.2 Mylar

As shown in Figure 10 for 3 mil thick Mylar there is no indication of any charging below 2 kV. Above 2 kV the drop in I_S/I_P indicates that the secondary emission coefficient is less than one causing a net buildup in negative charge. With the increase in surface charge the surface leakage current ratio I_R/I_P increases. For beam accelerations above 12 kV charge penetration is sufficient in combination with the space charge fields of trapped charges in the dielectric to cause conductivity. This conductivity is referred to as electron bombardment induced conductivity. Discharging and electroluminescence results from this tendency of the dielectric to hold a space charge. Throughout the 2 to 25 kV range the dominant electron loss from Mylar is by secondary electron emission.

Figures 11 through 14 are photo micrographs of a Mylar surface after 25 min of electron bombardment at 30 kV, 30 nA/cm^2. Damage is manifested as tracking and treeing. Table 7 summarizes the data for Figures 11 to 14.

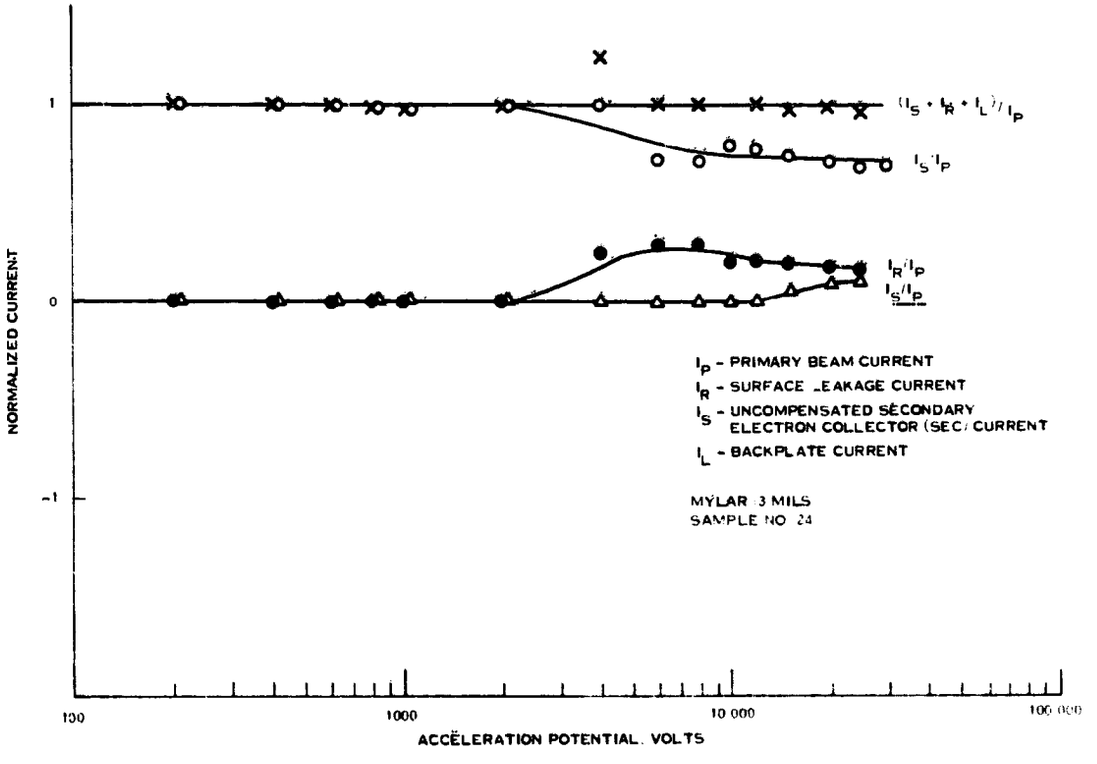

Figure 10. Charging Characteristics of Mylar Film (3 mils) at 30 nA/cm^2

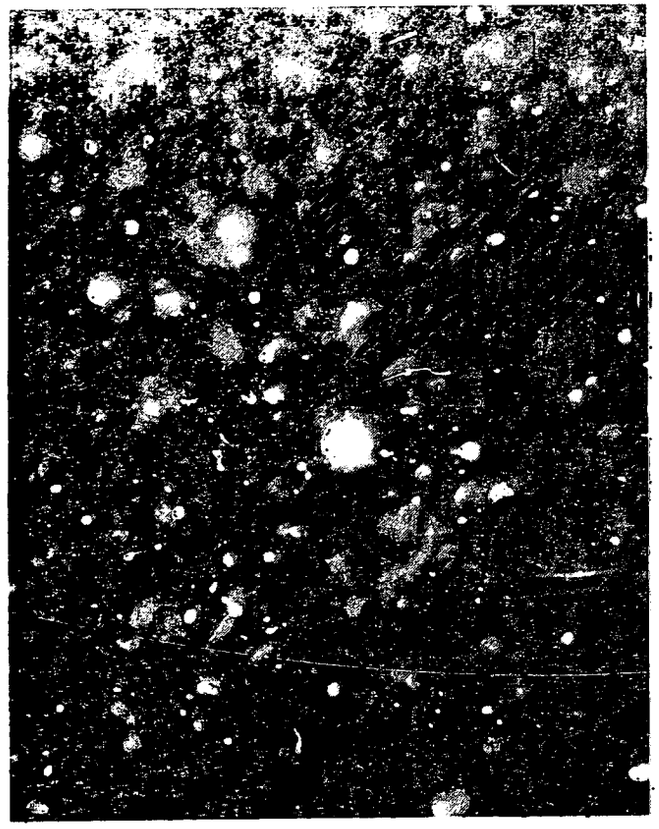

Figure 11. As Received Mylar (200×)
Dark Field Illumination

Figure 12. Electron Bombarded Mylar (100×)
Plain Polarized

Figure 14. Electron Bombarded Mylar (400×)
Plain Polarized

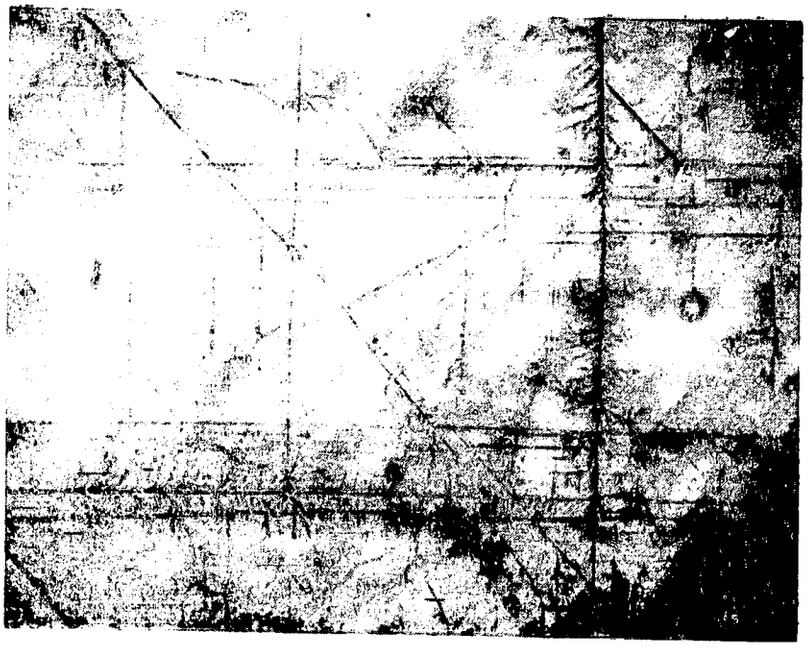

Figure 13. Electron Bombarded Mylar (200×)
Plain Polarized

Table 7. Data Summary for Figures 11 Through 14

	Sample No. 1	Sample No. 2A/B	Sample No. 3	Sample No. 4
Material	Mylar	Mylar	Mylar	Mylar
Thickness	0.003 in.	0.003 in.	0 003 in.	0.003 in.
Exposure	Room Illumination	Electron Beam	Electron Beam	Electron Beam
Voltage	---	30 keV	30 keV	30 keV
Current	---	30 nA/cm^2	30 nA/cm^2	30 nA/cm^2
Magnification	200X	100X	300X	~ 400X
Inclusions	~0.0001 in.	Present	Present	Present
Microscope Illumination	Dark Field	Plain Polarized	Plain Polarized	Plain Polarized
Aluminum back (not bonded)	None	Yes	Yes	Yes
Side Viewed	---	Electron Bombarded	Electron Bombarded	Electron Bombarded

No visual evidence of electric discharges could be seen (at 50X magnification) on the Mylar. However, at higher magnification brick pattern-treeing is evident, as illustrated by the photographs.

Brick pattern treeing, caused by electron beam irradiation etching, increases the surface energy of the Mylar by breaking bonds at and within a few microns of the surface. With respect to the treeing pattern, internal or frozen-in stresses may result from molecular orientation or from thermal stresses attributable to rapid cooling of the polymer. The intensity of the crazing increases with exposure time to electrons.

Apparently, large (micron size) structures of 500 to 1000 Å diameter spheres develop in the dielectric during the fabrication process, and lie in rows along the stretch direction of the polymer fibers. They represent the distribution of highly organized strain, due to fabrication stresses. The spheres, spatially ordered over a long period, are composed of highly ordered molecular groups (and crystallites) which may move as rheological identities. The tree patterns which develop over the strain pattern are due to surface electric discharges at the patterns. Correlation of physical properties (for example, % elongation, tenacity, tear, modulus) with structural size of brick pattern is apparently indicated, especially in the brick size of 1 to 100 μ. Strain distribution is an important parameter with respect to physical properties.

Laminar structure may also arise in stretched polymers due possible to anisotropic heat transfer during fabrication by anisotropic structures introduced into

the polymer. The regularity displayed by these structures indicates that the applied stress has been fairly uniform. In essence then, the parallel stretch direction lines and brick structure (unlike a grid structure, since the perpendicular lines, originating from parallel lines, do not generally cross adjacent parallel lines) are etched into one-way stretched polymer films. The number of lines are dependent upon the polymer history. In contrast, the two-way stretched polymer film etchings reveal lamellate composition, each layer having brick wall-like structure. Micron size bricks are apparently composed of spheres or groups of molecules of about 700 Å, aligned to a moderate extent. The electric discharge trees traverse paths of least resistance along the various higher energy strain trajectories of the brick pattern and to a lesser degree over the surfaces of the polymer. Some die lines also appear on the Mylar film along which the electric discharges traversed.

Mylar is not a commonly used external spacecraft material because of its sensitivity to the radiation components of the natural space environment which cause catastrophic degradation in its physical properties. The results of this investigation show that it is not suitable for use in a high electron flux environment, particularly when exposed directly to electron bombardment. However, its use in multilayer insulation (MLI/blankets) is acceptable where protected by a cover layer of a protective material such as Kapton or Teflon or any other material which will shield it from direct exposure.

5.3 In_2O_3/SnO_2 (ITO) Coating

Figures 15, 16, and 17 show the effects of the ITO semiconductor coating on the current/voltage characteristics of polymeric films. For both Kapton and Teflon substrates the secondary emission coefficient is greater than 1 for accelerating potentials below 4 kV. The aluminized backing shows no effect on the characteristic curves. The similarity between the curves for both Kapton and Teflon indicate the dominant effect of the semiconductor film with little effect on the crossover point between I_R and I_S for the two dielectrics. The rise in surface leakage current indicates low charge buildup on the surface of the dielectrics.

Micrographs of ITO (250 Å) coated FEP Teflon after electron beam irradiation are shown in Figure 18b indicating "electron-etched" cracking and crazing. These craze-cracks (due to large applied anisotropic stress or tensile force) run along parallel direction of stretch lines to which the material was subject (that is, longitudinal drawing or pulling and radial blowing), as is evidence by the micrograph of the unexposed spacecraft material (Figure 18a) and less evident outside the electron beam irradiation area (Figure 18c). The stretch lines correspond to the direction of molecular orientation, preferentially, since the polymer under the coating has less strength perpendicular to the direction of orientation. Crystallization occurs along these oriented molecules.

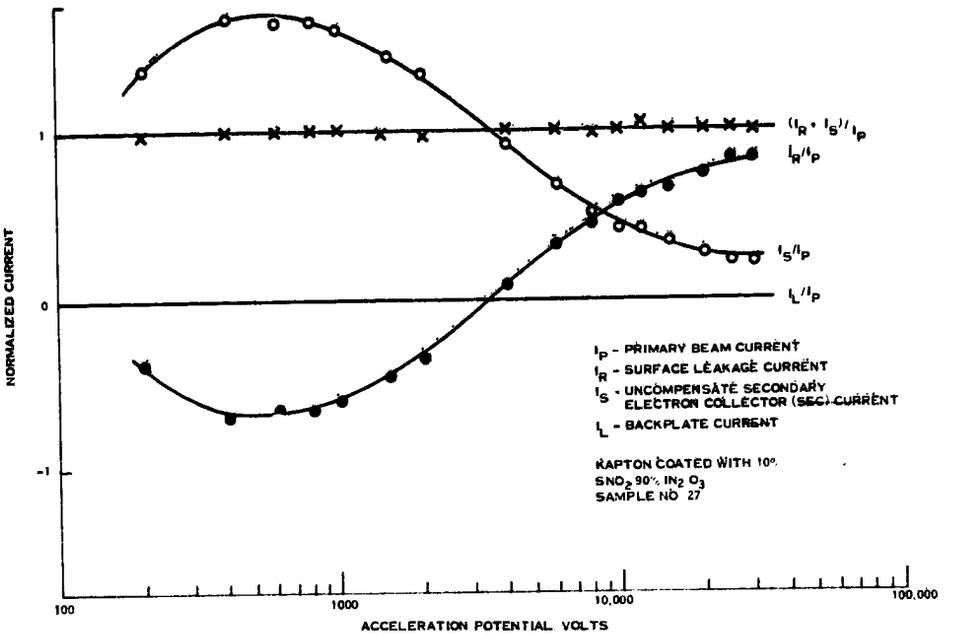

Figure 15. Charging Characteristics for ITO Coated Kapton Film at 30 nA/cm^2

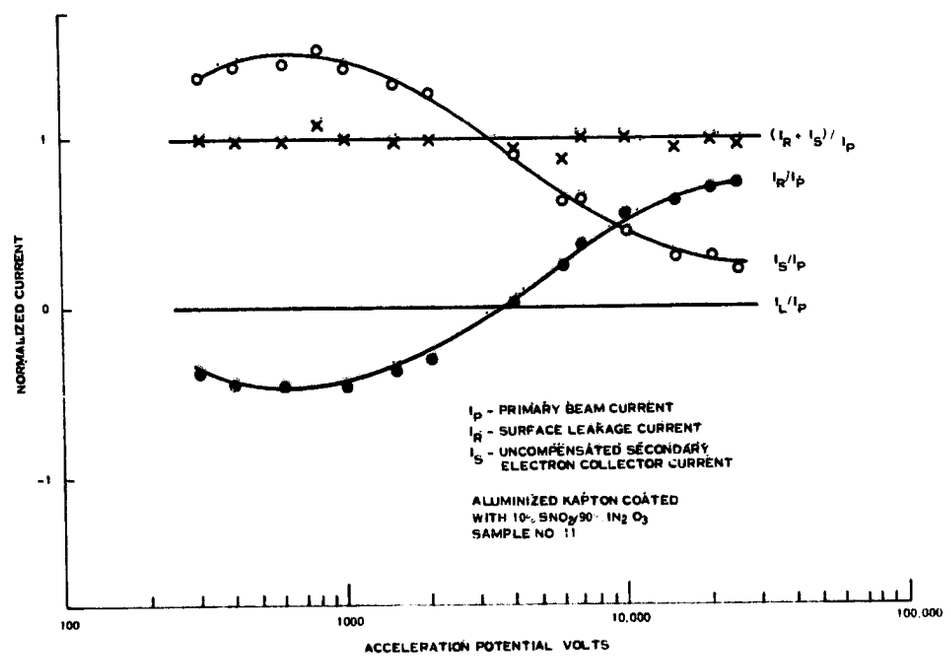

Figure 16. Charging Characteristics for ITO Coated Aluminized Kapton Film at 30 nA/cm^2

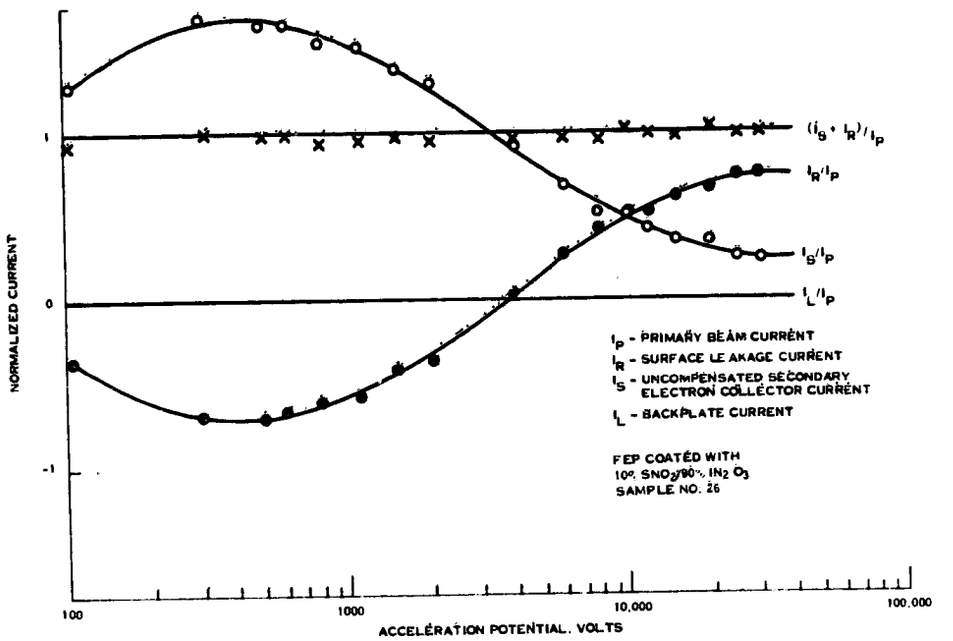

Figure 17. Charging Characteristics for ITO Coated FEP Film at 30 nA/cm^2

Within these imperfections and voids intrapped gas is ionized by electron beam charging. Local temperatures rise, chemical reactions occur and stress is created, as in the case of chemical or vapor etching.

Intensity of crazing rises with exposure time to the electron irradiation. Crazing of polymers apparently is related to domain structure of the polymer (that is, definite homogenous regions surrounded by others of like kind with boundaries between them). More craze lines form whenever the stretching occurred without lateral restraint than if the stretching occurred with lateral restraint for the same stretching ratio.

In essence, crack-crazing in polymers is associated with large micron size regular structures, which in general occur in anisotropically stretched (or uniform applied stressed) films. This structure is inherent in the film during the fabrication therefore a distribution of strain is produced by fabrication stress.

Figure 18b. FEP/ITO After Electron Irradiation at the Central Region of the Electron Beam. Electron etched craze lines appear on the FEP-Teflon surface, together with fabrication die lines, under the transparent semi-conductor (200X)

Figure 18a. Transparent Semi-Conductor of 250 Å Tin and Indium Oxide (10 percent mole SnO: 90 percent mole In_2O_3) on 2-mil FEP-Teflon Before Electron Irradiation. Typical die lines appear on the FEP-Teflon surface, under the transparent semi-conductor

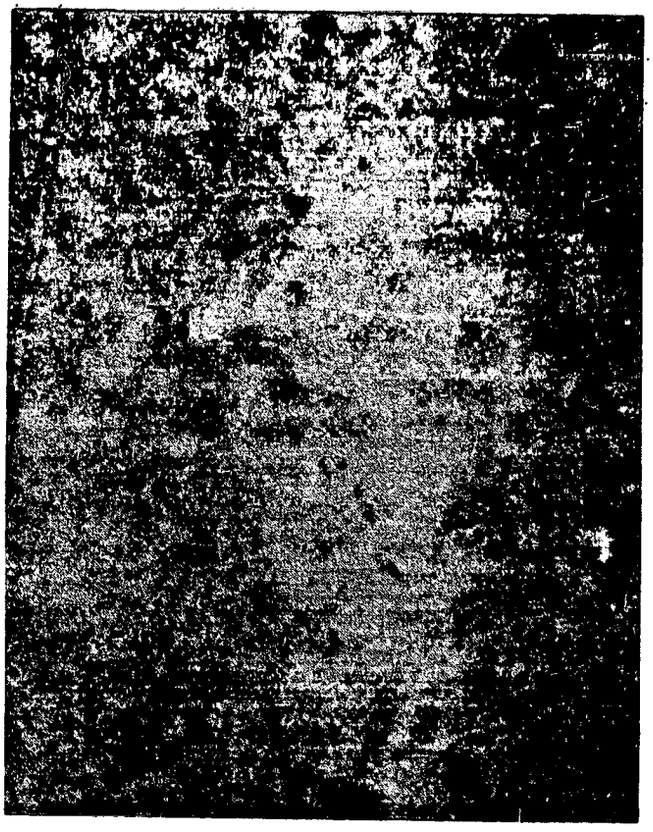

Figure 18c. FEP/ITO After Electron Irradiation Near the Edge of the Sample Outside the Primary Beam Projection Area

The micron size structure of "spheres" (500 to 1000 Å) denotes distribution of strain, due to fabrication stress. These "spheres" are highly ordered molecular groups and they move as rheological groups. The internal stresses may result from molecular orientation or from thermal stresses due to rapid cooling of the polymer. In the case of single way stretch in fairly evenly spaced long parallel lines of uniform width (for example, to 7μ) etched into the surface along the stretch path, the density of the lines (for example, number of lines per unit length) is apparently proportional to the stretch ratio, whereas the line width is proportional to the inverse of this stretch ratio.

5.4 Copper Grids

Figures 19 to 23 represent the characteristic curves for Teflon and Kapton substrates of various thickness with copper grids applied by a photoetching process. All of these curves show the same general behavior between 1 kV and 10 kV. As in the Mylar substrate the low value of I_R/I_P indicates a net charge buildup on the surface. Above 10 kV the penetration depth and charge buildup results in an increase in the electron bombardment conductivity. An anomolous behavior was observed in the 5-mil sample of Teflon, plain and aluminized, with the copper grid below 1 kV when the secondary current indicated a current ratio greater than 1 (Figure 20).

Comparison of the voltage-current characteristics of 2-mil Teflon (Figure 19) with 5-mil material (Figure 23) shows that the resistance of FEP increases with increased thickness. The relatively rapid rise of backplate leakage (through the sample) current, I_L, beyond 10 kV and the associated surface-currents, I_R, indicates the presence of micropores in the 2-mil thick film, some of which reach the backplate, as indicated by Malter avalanche emissions from these sites. This accounts for point emission distribution over the electron irradiated surface as a consequence of the associated spreading potential.

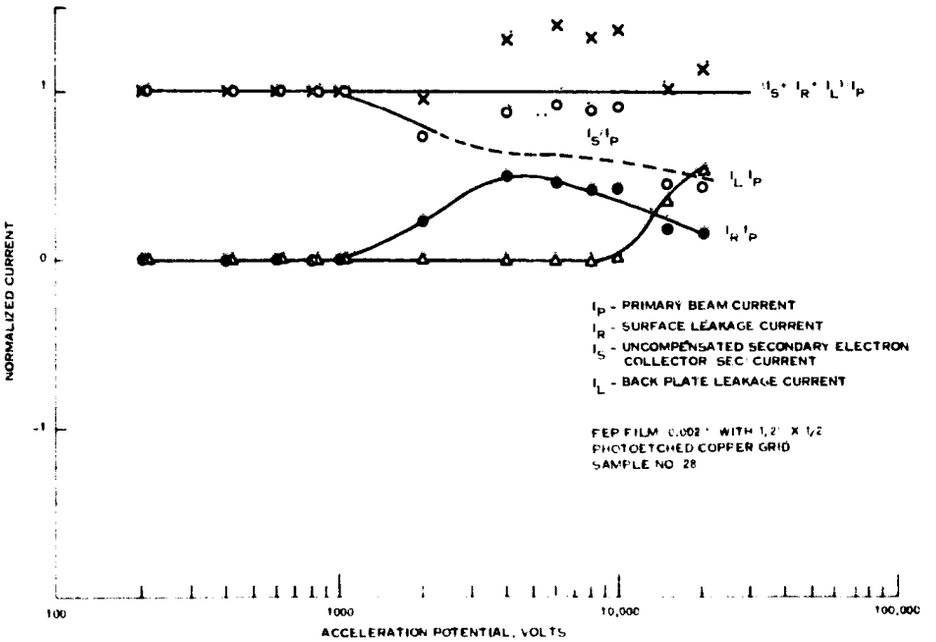

Figure 19. Charging Characteristics for 2-mil FEP With Photoetched Copper Grid at 30 nA/cm^2

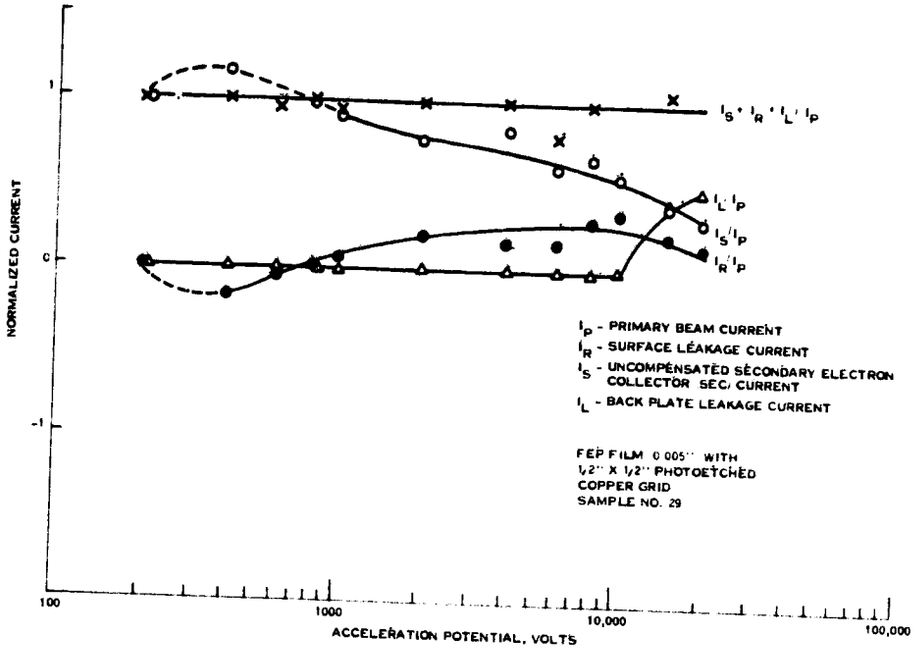

Figure 20. Charging Characteristics for 5-mil FEP With Photoetched Copper Grid at 30 nA/cm^2

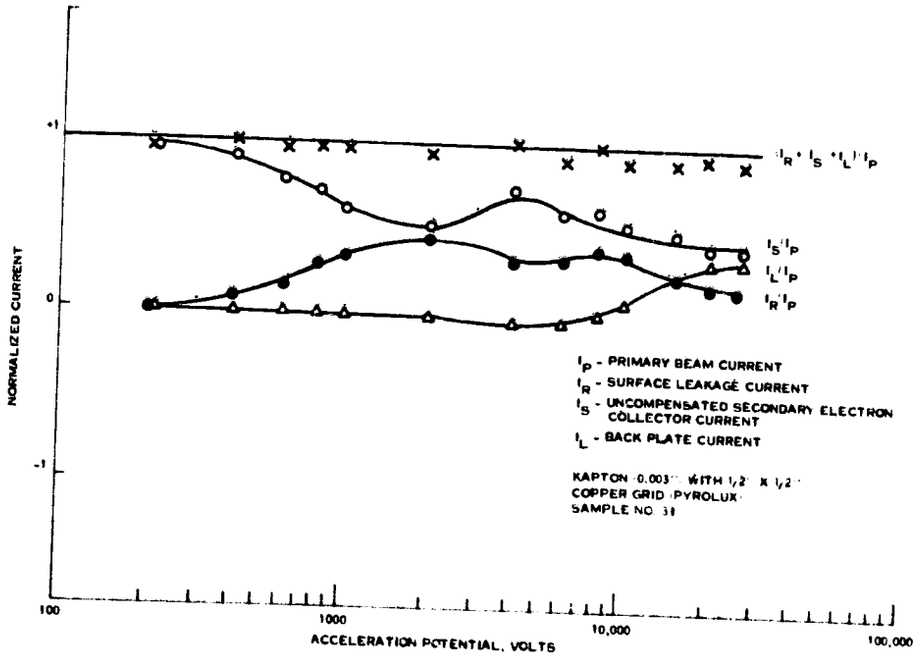

Figure 21. Charging Characteristics of Kapton Film (3-mil) With Photoetched (Pyralux) Copper Grid at 30 nA/cm^2

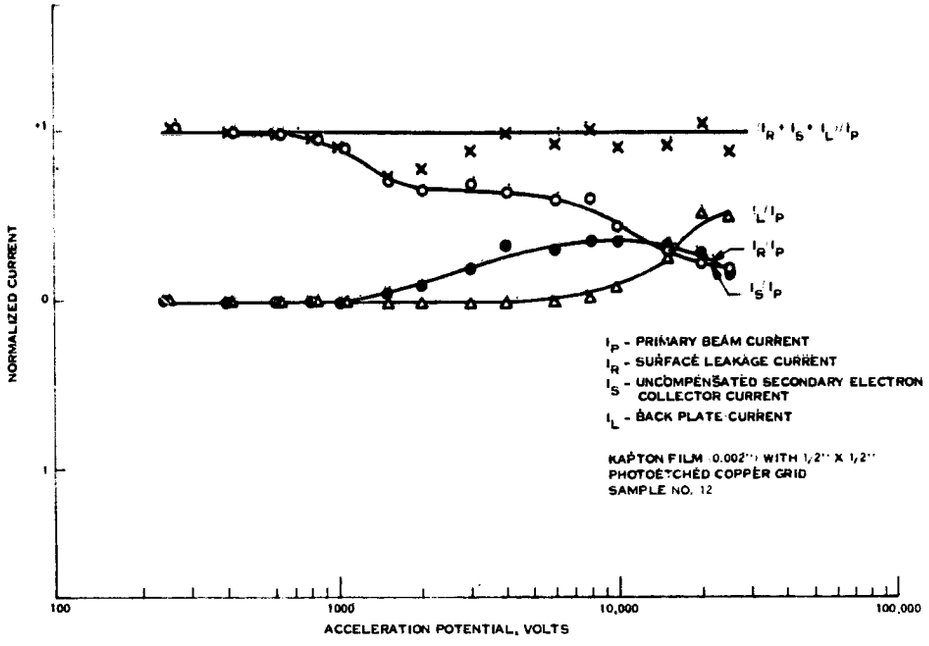

Figure 22. Charging Characteristics for Kapton Film (2-mil) With Photoetched Copper Grid at 30 nA/cm^2

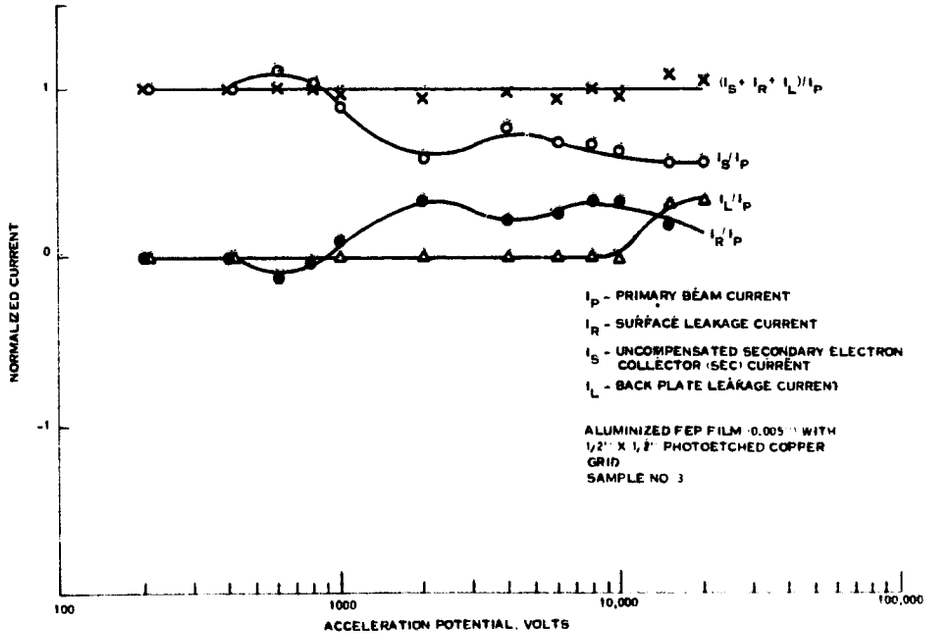

Figure 23. Charging Characteristics for Aluminized FEP Film (5-mil) With Photoetched Copper Grid at 30 nA/cm^2

Aside from the foregoing Malter avalanche emission, discharge breakdown in micropores of occluded gas in the Teflon can result in cavity ionization and thermal breakdown prior to intrinsic breakdown. This would account for some observed intermittent sparking observed. The moderate decreasing surface leakage current, I_R, beyond their respective peaks for both the 2- and 5-mil materials indicates that the residual gas surf- discharge threshold for the reduced charge (that is, ratio of surface charge to dielectric constant) as a function of dielectric resistivity has not been attained for the thicker film within the applied primary electron beam energy of 10 to $\geq$ 20 kV; whereas, it apparently did occur for the 2-mil material beginning about 15 kV. Examining the 2-mil Teflon at 10X magnification revealed that for the region displaying copious sparking, evidence of gaps in the copper grid occurred (Figure 24). Some filaments had as many as six very small gaps (order of a tenth of a millimeter) in one filament within the grid patch (that is, 12 in.). Some grid filaments had gaps on the order of millimeters wide, with no evidence of prior bonding in those gaps.

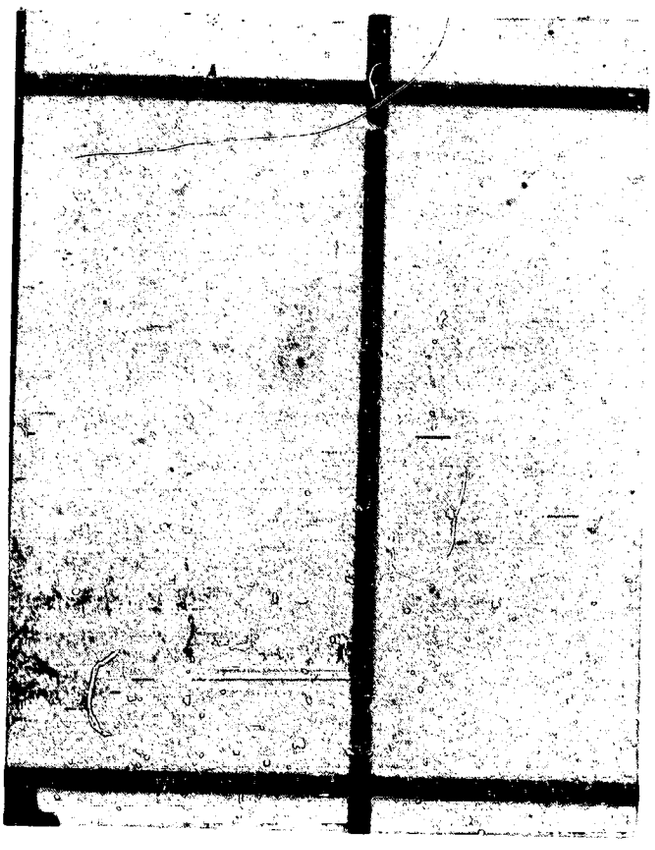

Figure 24. FEP Teflon (2-mil) Showing Discontinuities (As a Result of Electron Bombardment) in the Photo-etched Copper Grid Along Extrusion Lines in the Polymer

The unsatisfactory performance of this particular copper gridded Teflon is attributed to the numerous and small gaps in too many filaments of the grid. Uniformity of bonding is suspect, since no evidence of bonding occurs in the larger (several millimeters) wide gaps. The copper filaments themselves have clean distinct edges, with no raggedness, and of uniform, constant width. By electrically* increasing the surface energy of the Teflon, substantially improved bonding and absence of filament gaps is anticipated. Therefore, copper grid bond Teflon warrants improved processing and re-test.

Throughout the range of primary electron beam voltage, V_P, (> 200 to > 20 kV), the dominant electron loss from 5-mil FEP is by secondary electron emission as indicated by its I_S.

The surface leakage current, I_R, is relatively dominant, with respect to the backplate leakage current, I_L, from 850 V to 10 kV, whereas beyond this voltage (~ 12.5 kV) the backplate leakage current, I_L, assumes relative dominance over the surface leakage current, I_R.

The backplate leakage current, I_L, is relatively negligible, from about 200 V to about 10 kV and then rises abruptly approaching 15 kV. Near 30 kV, meters indicated electric discharging to be occurring at relatively frequent intervals (that is, 1 per 20 sec). However, actual electric discharging could not be seen on the sample in spite of several small (that is, $\ll 1/10$ mm) and a few substantially larger (that is, several mm) gaps in the copper grid filaments which were found during the post test microscopic examination.

5.5 Silk Screen Grid on Kapton

A net charge buildup is observed (see Figure 25) for accelerating potentials above 1 kV for 1-mil Kapton with a silk screen silver grid. Above 4 kV the surface leakage shows a decrease along with a faster decline in the secondary electron emission. Above 10 kV the predominant charge movement is by EBC indicating significant penetration into the dielectric substrate and large charge buildup on the surface.

The superior performance of the silk screened Kapton is evident from its voltage-current characteristics with respect to the substantial secondary electron emission (SEE) yield and backplate leakage current. In contrast, the surface leakage

---

*F-C bond breaking by electron irradiation or displacing sufficient F's by O's via microwave discharge, the surface energy of Teflon can be increased from 102° ± 4° (natural) to 65° ± 8° contact angle with a water vapor microwave discharge. The surface free energy, E_{SO}, of the dielectric relative to vacuum is related to the equilibrium contact angle, θ, by proportion: $E_{SO} \approx [1(1 + \cos\theta) + \pi_e]2$. The maximum reversible work of adhesion, Wa, of the two solid surfaces, S_1, S_2, in contact, is related to the contact angle, θ, by the proportion: Wa ≈ $(1 + \cos\theta)$, emphasizing only the contact angle among other intentionally undefined and omitted variables, for the interim.

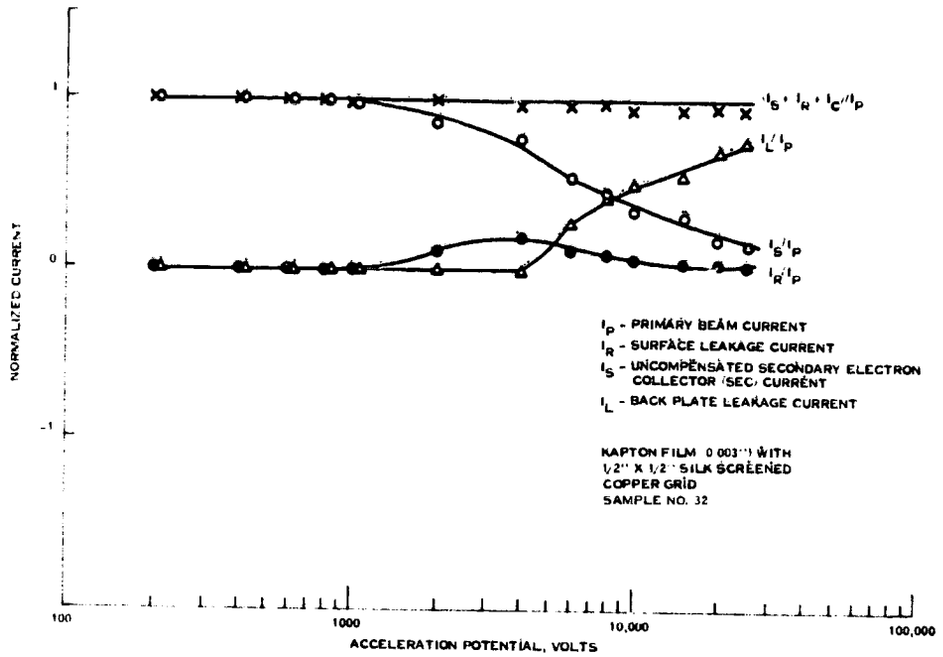

Figure 25. Charging Characteristics for Kapton Film (3-mil) With Silkscreened Copper Grid

current, I_R, although initially large, subsequently decreases rapidly, due to the rapid rise in backplate leakage current beyond 4 kV primary electron beam energy. Up to the latter voltage, the dominant electron current loss from this material is due to SEE current, I_S; and to a minor degree, surface leakage current, I_R, while the backplate current, I_L remained negligible. However, beyond a primary electron beam energy of 4 kV, the dominance of backplate leakage current, I_L, rapidly asserts itself. While the SEE current, I_S, relatively rapidly decreases, the backplate leakage current, I_L, becomes substantially dominant beyond 8 kV with respect to the SEE current, I_S, and surface leakage current, I_R.

Examination of the silver-grid bonded Kapton (at 10× magnification) reveals that the filaments of the grid are of fairly uniform width and deposition. They are uniformly well bonded to the Kapton. However, there are some regions of silver scarcity in that localized portions of some filaments have extremely thin (~ 1/10 width of filament) silver bridges connecting them, defects which must be remedied to obtain optimum performance. The surface of the silver filaments are relatively rough, though apparently this disadvantage does not cause localized discharges. Die marks are evident on the central regions of the Kapton windows of the grid (due

to processing. However, electron irradiation etching of the Kapton (bond breaking) is not obvious at 100× and 400× magnification (Figure 26). That is, no parallel single- nor double-way stretch (stress) patterns, nor brick-stress pattern is evident. This is apparently attributed to the charge dissipative ability of the grid in conjunction with significant electron bombardment induced conductivity in the Kapton, between the grid filaments, as well as the substantially lower resistance of the thin (1-mil) Kapton.

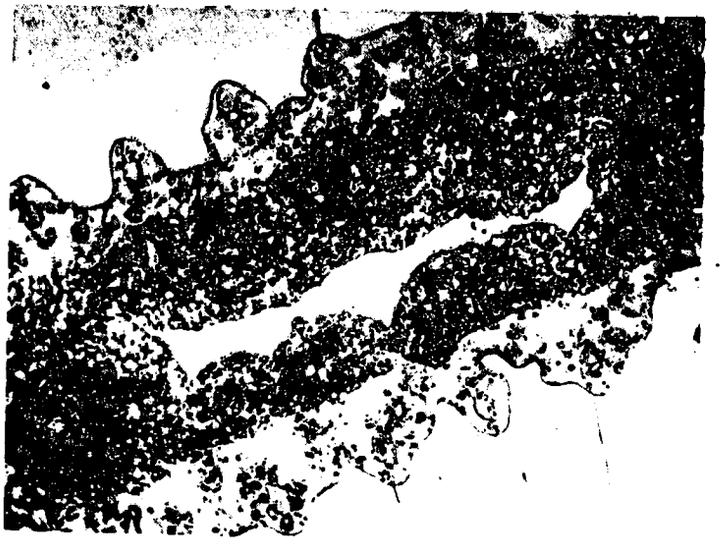

a. (100 ×) Grid Filament

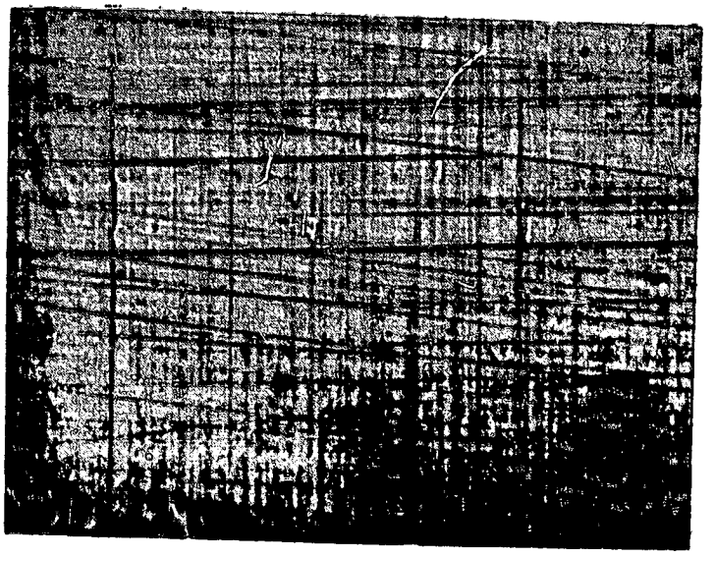

b. (400 ×) Kapton

Figure 26. Kapton Film (1-mil) With Silk Screened Silver Grid After Electron Bombardment

There were no measureable discharges for this material during electron bombardment through 25 kV and is apparently a satisfactory prospect for spacecraft thermal blanket application.

6. CONCLUSIONS

Mixtures of indium and tin oxides (90/10) reduce the surface resistivity of polymeric films sufficiently to control static charge buildup in simulated environmental tests. In this study a film thickness of only 250 Å was sufficient to attain a resistance in the 10^6 ohm-cm range without significantly reducing the visible transparency of FEP Teflon. No discharging occurred under electron bombardment to 25 kV with an associated current density as high as 30 nA/cm^2. The additional data needed to qualify this material for spacecraft use is that which will show reasonable stability in the space environment and resistance to damage by flexing the coated film.

On the first condition it is hypothesized that only slight discoloration of the ITO will occur under space UV and electron irradiation because of the thinness of the coating required ($\leq$ 250 Å) to obtain the conductivity to spread out the charge arising from solar substorms. This hypothesis is based on data taken on ITO coated OSR's produced by OCLI and Lincoln Laboratory in the GE Combined Effects Chamber in 1975 for the AFML Sponsored Thermal Control Coating Development Program.[3] A $\Delta\alpha_s$ of 0.01 was related to ITO coating during a EUVS exposure. The reason for the slight effect of the degrading ITO on the performance of the solar reflecting mirror is that the extinction coefficient is not only a function of the amount of light that is absorbed in the ITO, but also its thickness. A long term exposure to UV and low energy (few eV) particles (electrons and protons) which are deposited primarily in the conductive coating and FEP or disruption of the FEP surface during coating deposition will thereby reduce performance of the polymer under irradiation. These effects should be minimal using Magnetron equipment to deposit coatings because of the very low temperature rise which occurs during the deposition process.

Cracking or crazing of ITO films during flexing of the polymer substrate may or may not affect static charge control performance. Preliminary data indicates that this will not be a problem. Microcracks in an ITO coated Kapton film were observed (under a microscope) after vigorous flexing of the film. However, the sample showed no discharges, and in fact, performed as well as an unflexed specimen to 30 kV, 30 nA/cm^2.

Once these potential problem areas have been cleared, ITO can conveniently be deposited in quantities large enough for spacecraft systems using conventional roll-coating equipment.

Our preliminary evaluations indicate that conductive grids formed by photo-etching copper or silk-screening silver filled paint on Kapton to be effective in controlling discharging to 25 kV and 30 nA/cm^2. A square 1/2-in. grid pattern was used based on an analysis recently completed for AFML.[4] Optimization of the grid pitch can be done empirically. However, this item does not appear to be critical from a passive temperature control point of view because Kapton is not used for control of critical surfaces and in using 0.015-in. wide filmanets only 6 percent of the Kapton surface is covered by the grid.

Very poor performance was obtained from FEP Teflon with copper grids because of poor bonding of the grid to the polymeric film. A remedy to this situation is not apparent, because bonding can only be improved by etching the FEP surface and this has proven to significantly disrupt the UV stability of the FEP. Alternatively, heat sealing a wire grid into the Teflon surface is another approach, but it too is expected to affect the stability of the FEP film in radiation environments. This is a cause for concern because back surface metallized FEP is used for passive temperature control of critical surfaces where even minor changes in solar absorptance produce unwanted temperature increases.

Acknowledgments

We gratefully acknowledge the contributions made by consultant Dr. E. Okress for his assistance in designing the ESD test facility and in interpreting test data.

References

1. Knott, K. (1972) The equilibrium potential of a magnetospheric satellite in an ellipse situation, Planet. Space Sci., 2:1137-1146.
2. Nanewicz, J.E., et al (1976) Spacecraft charging studies of voltage breakdown processes on spacecraft thermal control mirrors, Program in Astronautics and Aeronautics, Vol. 47.
3. Eagles, A.E. (1975) Exploratory Development of Thermal Control Coatings, Technical Management Report for Contract F33615-74-C-5087.
4. Eagles, A.E. (1976) Conductive Coatings for Satellites, AFML-TR-76-233.